Available online at www.sciencedirect.com
ScienceDirect
Journal of the European Ceramic Society 27 (2007) 2095–2102
www.elsevier.com/locate/jeurceramsoc

# Fabrication of mullite-bonded porous silicon carbide ceramics by *in situ* reaction bonding

Shuqiang Ding [a,b], Sumin Zhu [c], Yu-Ping Zeng [a,*], Dongliang Jiang [a]

[a] *Shanghai Institute of Ceramics, Chinese Academy of Sciences, 1295 Dingxi Road, Shanghai 200050, China*
[b] *Graduate School of the Chinese Academy of Sciences, Beijing 100039, China*
[c] *Department of Materials Science and Engineering, University of Missouri-Rolla, Rolla, MO 65409, USA*

Received 17 December 2005; received in revised form 1 June 2006; accepted 5 June 2006
Available online 7 September 2006

**Abstract**

An *in situ* reaction bonding technique was developed to fabricate mullite-bonded porous silicon carbide (SiC) ceramics in air from SiC and α-$Al_2O_3$, using graphite as the pore-former. Graphite is burned out to produce pores and the surface of SiC is oxidized to $SiO_2$ at high temperature. With further increasing the temperature, the amorphous $SiO_2$ converts into cristobalite and reacts with α-$Al_2O_3$ to form mullite ($3Al_2O_3{\cdot}2SiO_2$). SiC particles are bonded by the mullite and oxidation-derived $SiO_2$ to obtain porous SiC ceramics. The reaction bonding behavior, open porosity, pore size distribution and mechanical strength of porous SiC ceramics were investigated as a function of the sintering temperature, forming pressure and graphite content. In addition, the phase composition and microstructure were also studied.


*Keywords:* Porous ceramics; Mullite; SiC

## 1. Introduction

Porous ceramics have been widely used as the filters, membranes, catalytic substrates, thermal insulation, gas-burner media, and refractory materials because of their superior properties, such as the low bulk density, high permeability, high temperature stability, erosion/corrosion resistance and excellent catalytic activity.[1–4] As an important and attractive branch of porous ceramics, porous SiC ceramics attracts more and more attention from material researchers owing to their low thermal expansion coefficient, high thermal conductivity and excellent mechanical properties.[5,6] However, it is hard to sinter SiC ceramics at moderate temperatures due to the covalent nature.[7] In order to realize the low-temperature fabrication of porous SiC ceramics, secondary phases may be added to bond SiC. Utilizing the oxidation-derived silica to bond SiC particles, Zhu and his coworkers prepared SiC reticulated porous ceramics.[8,9] In the same way, She et al. developed a unique oxidation-bonding technique for the fabrication of porous SiC ceramics[10,11] and the oxidation bonded porous SiC ceramics exhibit good thermal shock resistance owing to the microstructure with connected open pores.[12]

$SiO_2$ reacts with α-$Al_2O_3$ to form mullite at temperatures over 1410 °C.[13] Compared with $SiO_2$, mullite possesses higher melting point and lower oxygen diffusion coefficient. Therefore, porous SiC ceramics could exhibit better high temperature stability and oxidation resistance, if mullite, rather than silica, is selected as the bonding phase. Furthermore, the thermal expansion coefficient of mullite ($5.3 \times 10^{-6}$/K at 0–1000 °C) approximates to that of SiC ($4.7 \times 10^{-6}$/K at 0–1000 °C).[14] The thermal expansion match and good chemical compatibility between SiC and mullite ensures mullite bonded porous SiC ceramics with the excellent high-temperature strength and thermal shock resistance.

A suitable way to prepare mullite ceramics with low dimensional changes is the reaction bonding process, using SiC and α-$Al_2O_3$ as the starting materials, because the sintering-induced shrinkage is compensated by the SiC-oxidation-induced volume expansion. At high temperature, the surface of SiC is oxidized to $SiO_2$ and then the latter with high reactivity reacts with α-$Al_2O_3$ to produce mullite. SiC particles are bonded by the *in situ* formed mullite, to obtain mullite bonded SiC ceramics. As

* Corresponding author. Tel.: +86 21 52415203; fax: +86 21 52413903.
*E-mail address:* yuping-zeng@mail.sic.ac.cn (Y.-P. Zeng).

0955-2219/$ – see front matter © 2006 Elsevier Ltd. All rights reserved.
doi:10.1016/j.jeurceramsoc.2006.06.003

the pore-former, graphite is thermoset so the liquid phase does not appear during its oxidation in air, which ensures that the green bodies avoid the shrinkage resulting from the surface tension of the liquid phase as the pore former is heated. At the same time, the oxidation temperature of graphite (600–850 °C) is higher than that of other organic pore-formers (~100 °C for polyvinylbutyral (PVB) and ~270 °C for polymethyl methacrylate (PMMA)) so that SiC particles are oxidized partly before graphite is burn out completely. Therefore, the skeleton of the green bodies is kept intact by the residual graphite and oxidation-derived silica before mullite is formed.

The objective of this work is to fabricate mullite-bonded porous SiC ceramics from SiC and α-$Al_2O_3$, using graphite as the pore-former by the *in situ* reaction bonding process at relatively low temperatures. The *in situ* reaction bonding behavior, microstructural evolution, open porosity, pore size distribution and mechanical strength of porous SiC ceramics were investigated.

## 2. Experimental procedure

Table 1 lists the compositions of the raw materials used in this study. The graphite powders of 5.0, 10.0 and 20.0 μm were employed, respectively, as the pore-former to fabricate porous SiC ceramics with different porosity and pore size distribution. According to SEM analysis, the graphite particles are flat and the size distribution is not uniform.

SiC, α-$Al_2O_3$ and graphite were mixed at different volume ratios and ball-milled in ethanol for 24 h to obtain homogeneous slurries. After being dried in an evaporator and sieved through a 75-mesh screen, the mixed powder was bidirectionally pressed into the rectangular specimens of 4.5 mm × 10.0 mm × 50.0 mm under a certain pressure using a steel die. Compositions of the specimens used in this study are listed in Table 2. The specimens were heated to burn out graphite before 850 °C at a heating rate of 2 °C/min and then were sintered in air at 1400–1550 °C at a heating and cooling rate of 5 °C/min.

All samples were weighted before and after the sintering to estimate the oxidation degree of SiC particles. Open porosity was determined by the Archimedes method, where the distilled water was used as the liquid medium. Pore size distribution was characterized by the mercury porosimetry (Model Pore-Sizer 9320, Micromeritics, USA). Specimens were machined to the dimension of 3.0 mm × 4.0 mm × 36.0 mm to test the flexural strength via the three-point bending test (Model AUTOGRAPH AG-I, Shimadzu, Japan) with a support distance of 30.0 mm and a cross-head speed of 0.5 mm/min. Four specimens were tested to obtain the average strength. Phase analysis was conducted by X-ray diffraction (XRD), via a computer-controlled diffractometer (Model RAX-10, Rigaku, Japan) with Cu Kα radiation (wavelength of 1.5418 Å). Microstructure and morphology of porous SiC ceramics were observed by scanning electron microscopy (SEM) (Model JSM-5600LV, JEOL, Japan). Moreover, the oxidation behavior of graphite and SiC particles in air was evaluated by thermogravimetry (TG) (Model STA 449C, Netzsch, Germany) analysis.

Table 2
Compositions of the green bodies used in this study

| Mixture | SiC:$Al_2O_3$:graphite (vol.) | Average particle diameter of graphite (μm) | Graphite content (vol. %) |
|---|---|---|---|
| 1 | 2.1:1:0 | – | 0 |
| 2 | 2.1:1:0.9 | 10.0 | 22.5 |
| 3 | 2.1:1:1.2 | 10.0 | 27.9 |
| 4 | 2.1:1:1.5 | 10.0 | 32.6 |
| 5 | 2.1:1:1.8 | 10.0 | 36.7 |
| 6 | 2.1:1:1.2 | 5.0 | 27.9 |
| 7 | 2.1:1:1.2 | 20.0 | 27.9 |

## 3. Results and discussion

### 3.1. In situ reaction bonding behavior

The oxidation causes a weight loss for graphite but a weight gain for SiC. According to the TG analysis, graphite oxidation begins at ~600 °C and completes at ~850 °C but the oxidation of SiC particles occurs above ~750 °C before graphite oxidation is completed.[15] This means that the network structure of green bodies can be stabilized by the residual graphite or the oxidation-derived $SiO_2$ before mullite is formed.

Graphite is oxidized to form gaseous CO or $CO_2$ above 600 °C, depending on the amount of oxygen in furnace. Since graphite oxidation occurs at 600–850 °C, the specimens should be heated before 850 °C at a low heating rate to ensure the slow release of CO and $CO_2$. Before the beginning of the mullitization between oxidation-derived $SiO_2$ and α-$Al_2O_3$, the amorphous $SiO_2$ transforms partly to cristobalite. According to the XRD

Table 1
Powder compositions and characterization of materials used in this study

| Material | Average particle diameter (μm) | Purity (wt.%) | Impurity (wt) | Resource |
|---|---|---|---|---|
| α-SiC | 20 | 99.4 | 0.24%$Fe_2O_3$, 0.12%MgO, 0.08%$SiO_2$, 0.06%$V_2O_5$, 0.06%C, 0.04%NiO | Weifang Kaihua Silicon Carbide Micropowder Co. Ltd., Weifang, China |
| α-$Al_2O_3$ | 0.6 | 99.9 | 0.03%$SiO_2$, 0.02%$SO_3$, 0.02%MgO, 0.01%$Fe_2O_3$, 0.01%$Y_2O_3$, 0.01%NaCl | Wusong Chemical Fertilizer Factory, Shanghai, China |
| Graphite | 5.0, 10.0, 20.0 | 99.9 | 0.04%NOi, 0.03%$SiO_2$, 0.03%$Fe_2O_3$ | Qingdao Huatai Lubricant Sealling Science and Technology Co. Ltd., Qingdao, China |

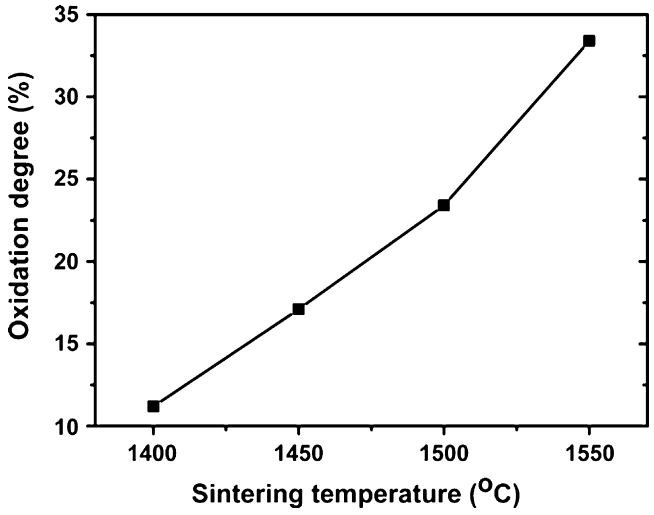


Fig. 1. Plot of oxidation degree of SiC vs. sintering temperature for the samples sintered at indicated temperatures for 4 h in air, where the 10.0 μm graphite was used, the volume ratio of SiC, α-$Al_2O_3$ and C in green bodies was 2.1:1:1.2 and the forming pressure of green bodies was 30 MPa.

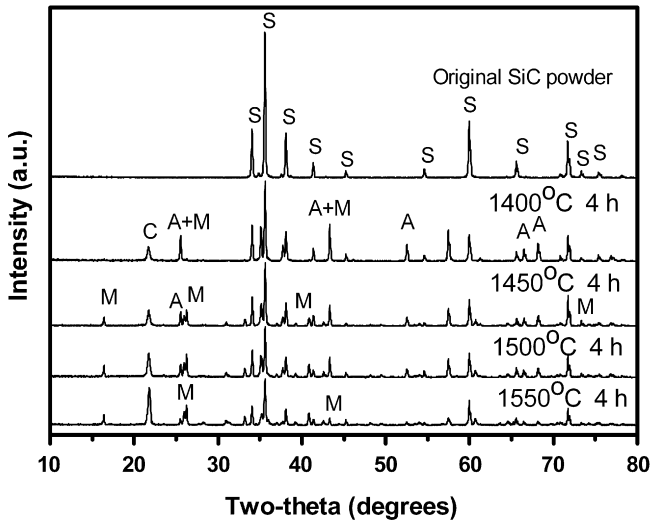


Fig. 2. XRD patterns of the specimens sintered in air, where the 10.0 μm graphite was used, the volume ratio of SiC, α-$Al_2O_3$ and C in green bodies was 2.1:1:1.2 and the forming pressure of green bodies was 30 MPa (S is SiC, M is mullite, C is cristobalite and A is α-$Al_2O_3$).

analysis of the SiC particles oxidized at different temperatures, the amorphous $SiO_2$ crystallizes to cristobalite above 1100 °C.[15] Cristobalite can enhance the bonding between SiC particles and improve the strength of porous SiC ceramics. However, excessive cristobalite is harmful to the high-temperature properties of porous SiC ceramics because of its large coefficient of thermal expansion ($17.5 \times 10^{-6}$/K at 20–700 °C).[14] Fig. 1 shows the plot of SiC oxidation degree versus sintering temperature during the fabrication of porous SiC ceramics. The oxidation degree increases from 11.2% to 33.4% with elevating the sintering temperature from 1400 to 1550 °C. The oxidation rate of SiC follows a parabolic law and the oxidized products are amorphous silica or cristobalite, depending on the temperature.[16,17] At the early stage of the SiC oxidation, $O_2$ diffuses to the surface of SiC easily and the oxidized products are $SiO_2$ and $CO_2$. As oxidation continues, the thickening of $SiO_2$ film and the formation of a mullite layer prevent or slow down the oxygen diffusion. This results in the lack of $O_2$ so that the oxidized products are gaseous SiO and CO. When these gases are given off, small pores are formed on the surface of SiC particles.

Fig. 2 shows the XRD patterns of porous SiC ceramics sintered at different temperatures for 4 h. At 1400 °C, porous SiC ceramics consist mainly of SiC, cristobalite and α-$Al_2O_3$, but slight mullite peaks can be found. When the sintering temperature increases to 1450 °C, the mullite peaks are obvious. At 1500 and 1550 °C, the amount of α-$Al_2O_3$ decreases abruptly and more extensive mullitization occurs. According to the $SiO_2$–$Al_2O_3$ equilibrium phase diagram,[18] mullite is formed from cristobalite and α-$Al_2O_3$ above 1400 °C. The mullitization between $SiO_2$ and α-$Al_2O_3$ can be explained by the solution-precipitation mechanism.[19,20] $SiO_2$ does not form a viscous liquid phase at 1400 °C but shows viscous softening. Due to the superficial softening, the fine α-$Al_2O_3$ particles penetrate into the viscous $SiO_2$ glass, leading to the nucleation of mullite. At 1450 °C, the viscosity of $SiO_2$ glass decreases and more $Al^{3+}$ ions are dissolved into the viscous $SiO_2$ glass. Above 1500 °C, the mullite formation occurs by the reaction between cristobalite and α-$Al_2O_3$. Because of the short diffusion distances achieved by viscous-flow-assisted sintering,[21] the rate of mullitization is accelerated drastically. After enough mullite is formed, the interfaces of $SiO_2$-mullite and $Al_2O_3$-mullite appear. $SiO_2$ and α-$Al_2O_3$ interdiffuse across the mullite layer and the formation of mullite is diffusion-controlled.

### 3.2. Microstructural evolution

Fig. 3 shows the typical microstructure of as-fabricated porous SiC ceramics sintered at 1500 °C for 4 h. It exhibits a stable structure with obvious connected pores and the well-developed necks appear between SiC particles. Though mullitization occurs in porous ceramics, the densification does not appear due to the mullitization prior to the densification,[22] result-

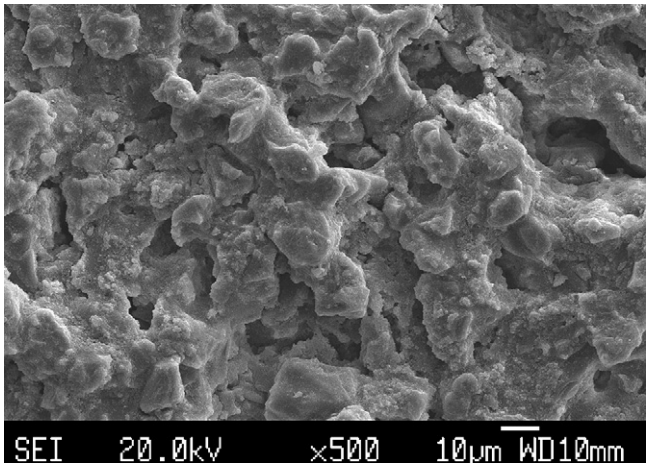


Fig. 3. SEM micrograph of porous SiC ceramics sintered at 1450 °C for 4 h in air, where the 10.0 μm graphite was used, the volume ratio of SiC, α-$Al_2O_3$ and C in green bodies was 2.1:1:1.2 and the forming pressure of green bodies was 30 MPa.

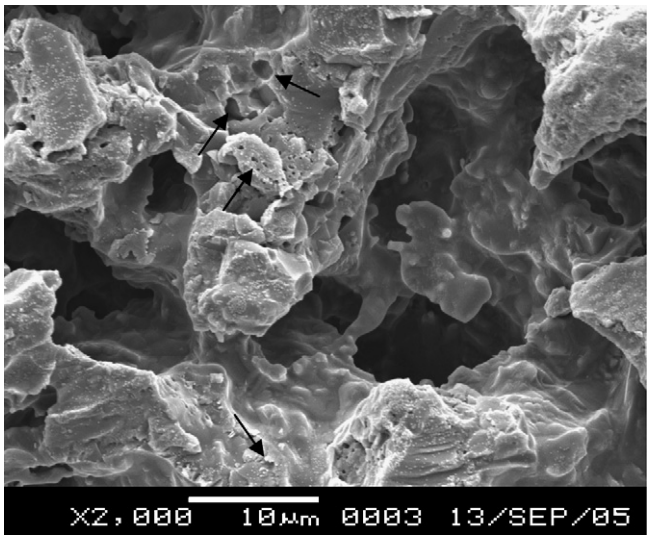


Fig. 4. Pores caused by the gaseous SiO and CO during the heating in porous SiC ceramics.

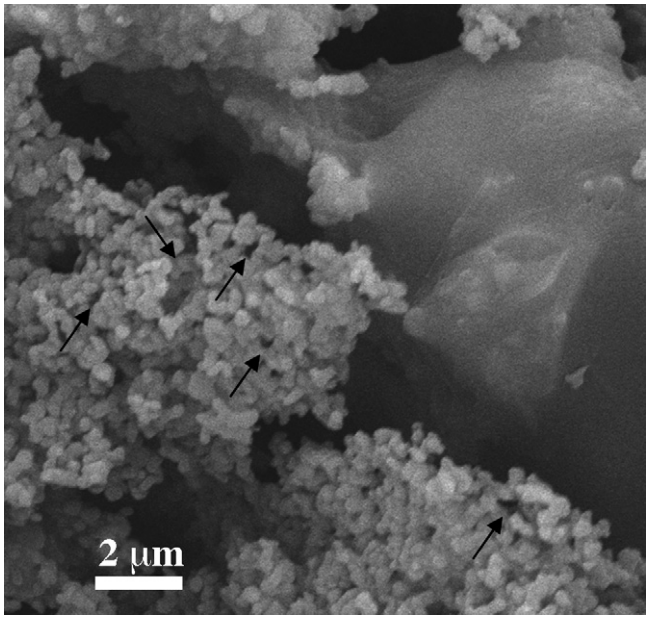


Fig. 5. Pores formed by stacking α-$Al_2O_3$ particles in porous SiC ceramics.

ing in the structure with plenty of open pores. The pores are mainly derived from both burning out graphite and stacking SiC particles. Since 20.0 μm SiC and 10.0 μm graphite are used as the starting materials, the pores originating from the burnout of graphite are larger than those originating from stacking SiC particles. Moreover, the number of large pores increases linearly with the graphite content because the place of graphite particles is substituted for the voids after they are burned out. Even smaller closed pores were observed in Fig. 4. This kind of pores is attributed to the further oxidation of SiC particles during the sintering. Although oxygen can diffuse into the outer of SiC particles, gaseous oxidation products (SiO, CO) are trapped in the oxidation-derived silica layer and cause the formation of bubbles.[23] In addition, small quantities of pores are formed by stacking residual $Al_2O_3$ particles which can not touch SiC particles homogeneously and then do not reacts with $SiO_2$ completely, as shown in Fig. 5. From the literature,[24] the continuous network may percolate from one side of the volume to the other at an inclusion volume of ≥22%. In the present work, the volume fraction (between 22.5 and 36.7 vol.%) of graphite added in the green bodies is beyond the threshold value. Thus, the pores from the burnout of graphite are mostly connected with each other.

According to the work by Obadia and Broussaud,[25] $Al_2O_3$ reacts with $SiO_2$ to form needlelike mullite at 1500 °C when the weight ratio of $Al_2O_3$ and $SiO_2$ is 4:6. Fig. 6 shows the needlelike mullite at the necks of porous SiC ceramics. Needle-like clustered grains of mullite were also observed on the surface of SiC. The firm struts between particles are formed because of the mullitization. It is considered that the porous structure is stabilized by the cristobalization and mullitization rather than the coarsening of SiC grains. Though the oxidation of SiC and the cristobalization are accompanied with the large volume expansion, microcracks were hardly observed and near-net-shape sintered samples with ±1.5% linear variation were obtained. It can be explained by the fact that the reaction-induced volume expansion is compensated by the sintering-induced shrinkage.

### 3.3. Open porosity and pore size distribution

Fig. 7 shows plots of open porosity versus sintering temperature, forming pressure and graphite content. Open porosity decreases with sintering temperature and forming pressure, but increase with graphite content. According to the theoretic calculation, a 108.2% volume expansion is associated when SiC is oxidized to cristobalite; further mullitization between α-$Al_2O_3$ and cristobalite only results in the volume shrinkage of 3.8%; and it is therefore expected that the total volume expansion is 37.3% when 2 mol α-SiC is oxidized completely in air and then reacts with 3 mol α-$Al_2O_3$ to form 1 mol mullite; assuming that the density of SiC, α-$Al_2O_3$, cristobalite and mullite is 3.22, 4.02, 2.32 and 3.16 g/cm$^3$, respectively. However, the dimen-

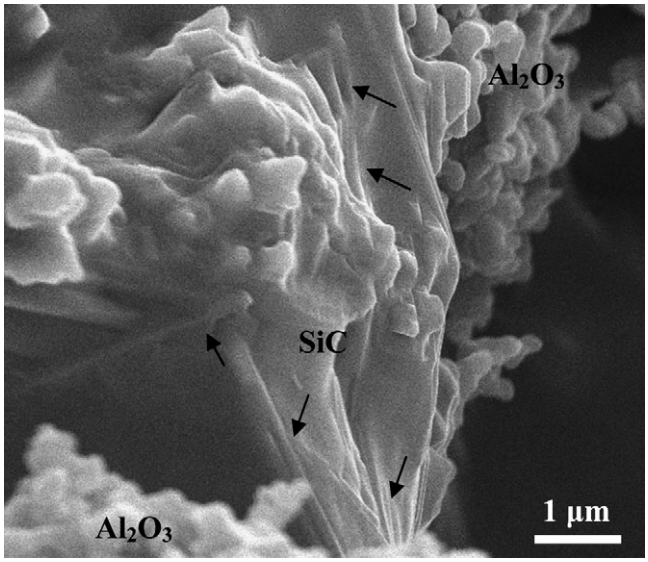


Fig. 6. Needlelike crystalline mullite at the necks of porous SiC ceramics sintered at 1450 °C for 4 h in air.

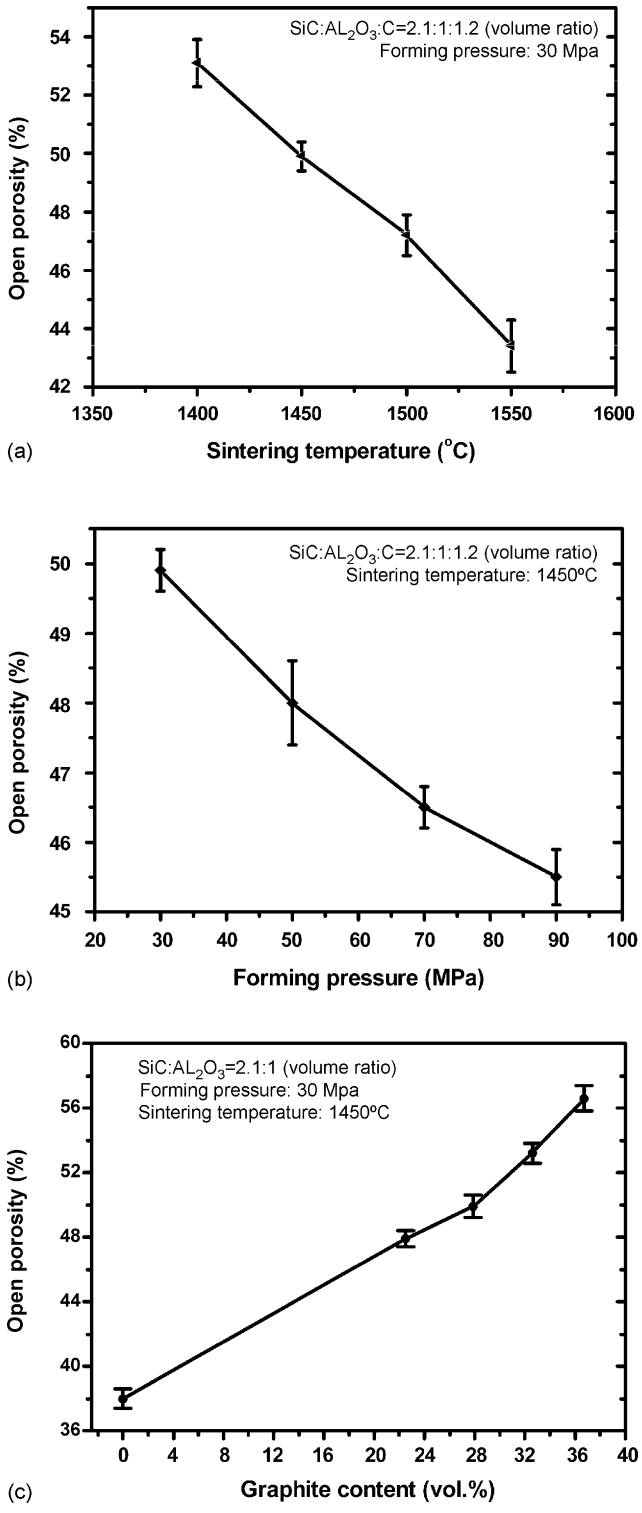


Fig. 7. Plots of open porosity vs. (a) sintering temperature, (b) forming pressure and (c) graphite content; the specimens were sintered at indicated temperatures for 4 h in air, where the 10.0 μm graphite was used as the pore-former.

sion of the specimens is almost invariable before and after the sintering though the oxidation and mullitization become sharper with increasing the sintering temperature. This phenomenon is attributed to the fact that the volume expansion part moves into the pores and then decreases the open porosity. In addition, higher temperatures result in more oxidation-derived $SiO_2$ with low viscosity, which may flow into the pores to reduce the open porosity. Large forming pressure makes the specimens compacted, increases the density of the green bodies and shortens the gaps between SiC particles. Further, the possibility of the closure of those pores by stacking SiC particles becomes large during the sintering because the shorter distance between SiC particles results in the smaller pores. Thus the open porosity decreases with increasing the forming pressure, as shown in Fig. 7(b). Graphite content has a significant effect on the open porosity of porous SiC ceramics. Fig. 7(c) shows that the open porosity increases with the graphite content. Porous SiC ceramics without graphite addition possess the open porosity of 38.0%, but the open porosity increases to 56.6% when the 36.7 vol.% graphite is added for mixture 5 in Table 2. It is shown that the open porosity is mainly contributed by stacking particles. The addition of 36.7 vol.% graphite only leads to a 18.6% increase in the open porosity because graphite particles with wide particle size distribution were partly dispersed into the voids among SiC particles.

Fig. 8 shows the pore size distribution of porous SiC ceramics with the graphite addition of different particle size. Porous SiC ceramics take on a narrow pore size distribution. When graphite particle size increases from 5 to 20 μm, the pore size distribution experiences a transition from a unimodal to bimodal distribution. In the curve with the bimodal distribution, the former peak (pore diameter = 1.6 μm) corresponds to the pores formed by stacking SiC particles and the latter (pore diameter = 8.0 μm) corresponds to those derived from burning out graphite particles. Since 20.0 μm SiC particles were used, the size of the pores by stacking SiC particles should be ∼8.3 μm theoretically, provided that spherical SiC particles are in the dense cubic (face centered cubic, FCC) stack. When the graphite particles of 5.0 and 10.0 μm were used, the size of the pores by burning out graphite approximates to that of the pores by stacking SiC particles so that there is no remarkable difference between them in the curves. While the graphite particle size increases to 20.0 μm, the pores from the burnout of graphite are much larger than those from the stacking of SiC particles (∼8.3 μm), resulting in the bimodal distribution of the pore size. Furthermore, it can be deduced from the curves that the average size of the pores by stacking SiC particles is ∼1.6 μm. This value is not consistent with the theoretical calculation (∼8.3 μm) according to the dense cubic stack of SiC particles, which should be attributed to the irregular shape and wide particle size distribution of SiC particles, the volume variation during the reaction bonding and the viscous flow of the oxidation-derived silica at high temperatures.

### 3.4. Flexural strength

Porous ceramics with high porosity fail abruptly at the stress which is far below the strength of the bulk material but the failure is non-catastrophic because the pores arrest the extension of microcracks.[26] Local failure of single strut does not necessarily cause the failure of the whole material. When the load is transferred to the neighbored pores, the progressive fracture occurs. As is shown in Fig. 9, porous SiC ceramics are usu-

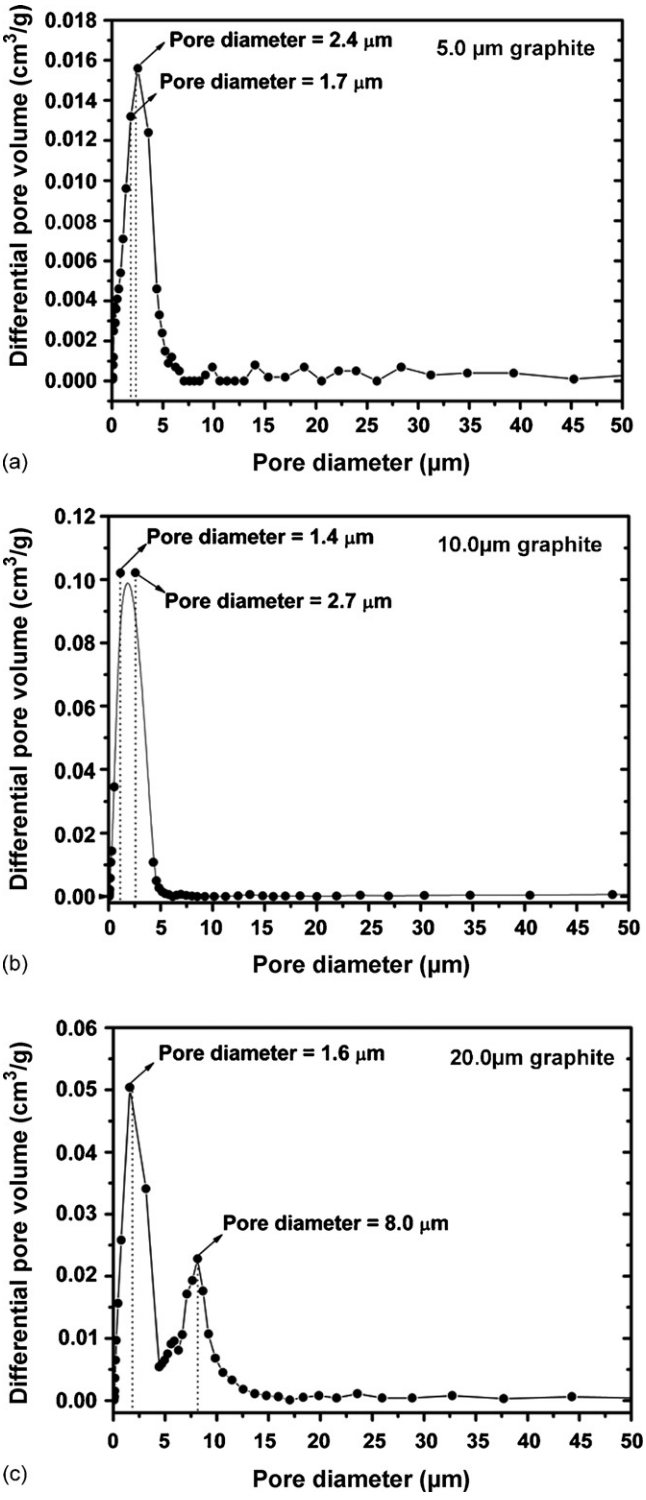


Fig. 8. Pore size distribution of porous SiC ceramics with the addition of the graphite of (a) 5.0 μm, (b) 10.0 μm and (c) 20.0 μm; the specimens were sintered at 1450 °C for 4 h in air, where the volume ratio of SiC, α-$Al_2O_3$ and C in green bodies was 2.1:1:1.2 and the forming pressure of green bodies was 30 MPa.

ally fractured along the necks between particles when the necks are weak compared with the surrounding particles. It exhibits discrete and non-colinear crack propagation.

The mechanical strength of porous SiC ceramics depends strongly on their microstructure. For porous SiC ceramics, the

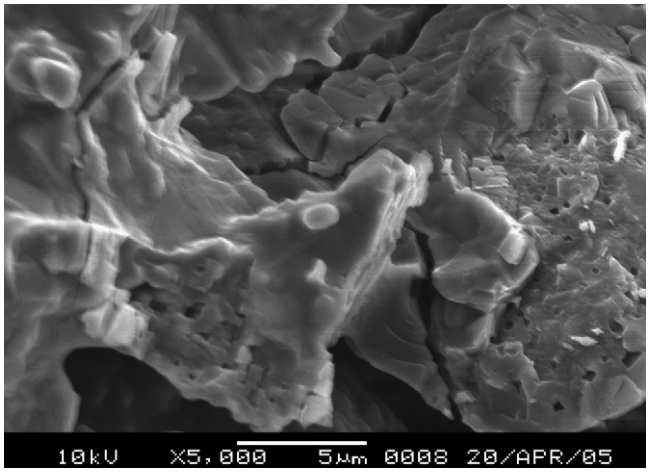


Fig. 9. Microcracks at the necks when porous SiC ceramics are fractured.

factors affecting the strength includes the grain size, bonding necks between particles, porosity, pore size distribution, pore shapes and flaws. In this work, the effect of the grain size, pore size distribution, pore shape and flaw on the mechanical strength is considered to be the same because of the same raw materials and processing adopted. The variable factors are only the porosity and the bonding necks. The porosity depends on the sintering temperature, forming pressure and graphite content, while the bonding necks could be reflected from the densification of porous SiC ceramics. The previous works[27–29] have shown that the mechanical strength of porous ceramics can be evaluated by the minimum solid cross-sectional area or the load-bearing area. Porous ceramics with further neck growth and lower porosity possess larger minimum solid cross-sectional area and then higher flexural strength.

Fig. 10 shows plots of flexural strength as functions of sintering temperature, forming pressure and graphite content. When the sintering temperature increases from 1400 to 1550 °C, the flexural strength is improved from ∼5.1 to ∼24.0 MPa. The flexural strength increases slightly with the forming pressure but decreases abruptly with the graphite content. As the sintering temperature increases, the oxidation of SiC, crystallization of the amorphous $SiO_2$ and the subsequent mullitization are accelerated. These changes augment the neck area between SiC particles and promote the bonding between SiC particles. Additionally, higher sintering temperature results in more silica with low viscosity and then reduces the porosity of porous SiC ceramics. According to the formulation of the strength–porosity dependence by Rice:[27–29]

$$\sigma = \sigma_0 \exp(-bp) \quad (1)$$

where $\sigma_0$ is the strength of a nonporous structure, $\sigma$ the strength of the porous structure at a porosity $p$, and $b$ is an empirical constant, the strength of porous ceramics takes on an exponential increase with the decrease of the porosity. As a result, the flexural strength of porous SiC ceramics increases with the sintering temperature. Higher forming pressure shortens the gaps between particles and reducing the porosity. The shortened gap facilitates the diffusion of α-$Al_2O_3$ to silica and accelerates the formation

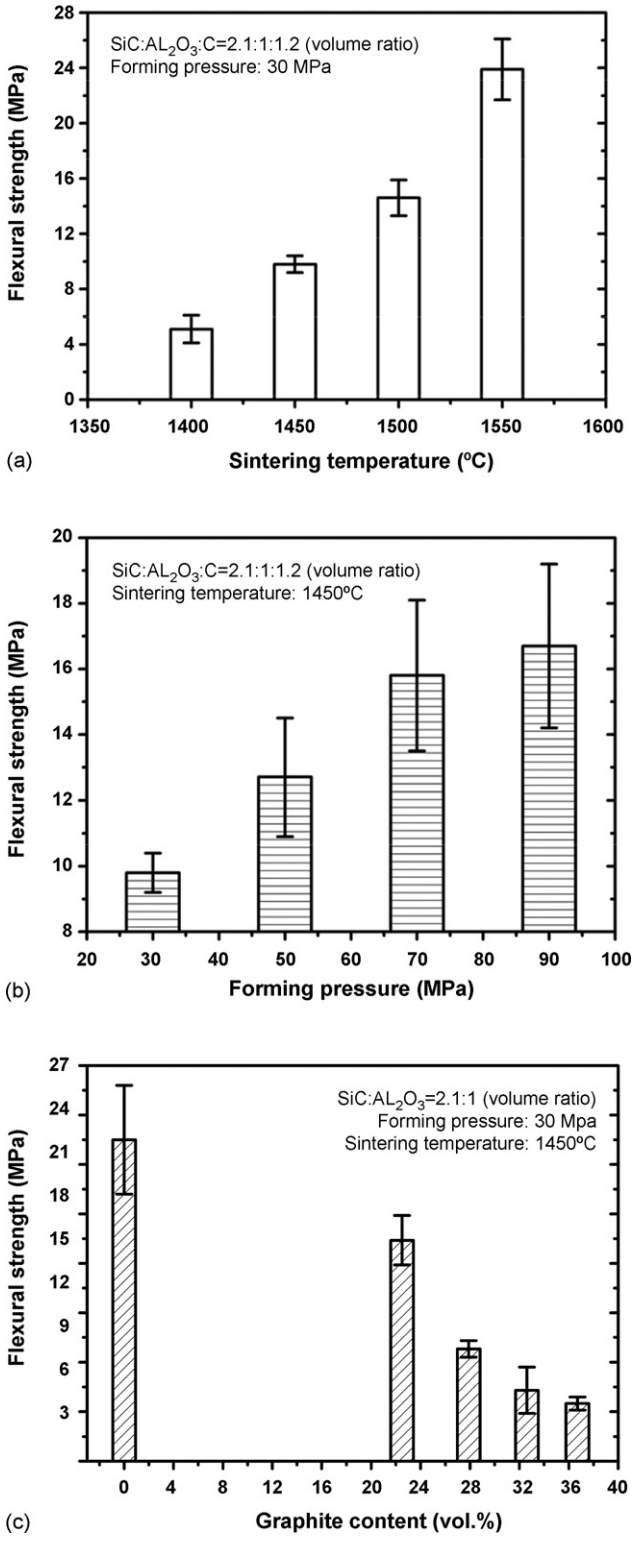


Fig. 10. Relationships of flexural strength vs. (a) sintering temperature, (b) forming pressure and (c) graphite content; the specimens were sintered at indicated temperatures for 4 h in air, where the 10.0 μm graphite was used as the pore-former.

of mullite, leading to the well-developed necks between SiC particles. Therefore, the flexural strength of porous SiC ceramics is improved as the forming pressure increases. Since graphite particles are burn out to produce pores, more graphite added in green bodies increases the porosity of porous SiC ceramics. The increase of the porosity reduces the load-bearing area when porous SiC ceramics are fractured, which results in the decrease of the flexural strength, as shown in Fig. 10(c).

## 4. Conclusions

Mullite bonded porous SiC ceramics were fabricated at 1400–1550 °C in air by the *in situ* reaction bonding technique. The needle-like clustered mullite crystalline was observed by SEM. Porous SiC ceramics are bonded by the mullite and oxidation-derived $SiO_2$. The pores are mainly derived from the burnout of graphite and the stacking of SiC particles. The average size of the pores by stacking SiC particles is ~1.6 μm, while the size of those derived from the burnout of graphite depends on the size of graphite particles. The open porosity decreases with sintering temperature and forming pressure, but increase with graphite content. However, the flexural strength is in direct proportion to the sintering temperature and forming pressure, but in inverse proportion to the graphite content. Due to the enhancement of necks between SiC particles, the flexural strength of 24.0 MPa was achieved at an open porosity of 43.4%.

## Acknowledgement

The authors would like to thank the "Plan of Outstanding Talents" of Chinese Academy of Sciences for the financial support.

## References

1. Green, D. J. and Colombo, P., Cellular ceramics: intriguing structures, novel properties, and innovative applications. *MRS Bull.*, 2003, **28**(4), 296–300.
2. Greil, P., Advanced engineering ceramics. *Adv. Mater.*, 2002, **14**(10), 709–716.
3. Gibson, L. J., Cellular solids. *MRS Bull.*, 2003, **28**(4), 270–271.
4. Woyansky, J. S. and Scott, C. E., Process of porous ceramics. *J. Am. Ceram. Soc. Bull.*, 1992, **71**(11), 1674–1682.
5. Brockmayer, J. W. and Dore, J. E., US Patent 4,885,263, 1989.
6. Rojas, P. C., Piderit, G. J. and Toro, P., Development of open-pore silicon carbide foams. *Key Eng. Mater.*, 1997, **132–136**, 1731–1734.
7. Riedel, R., Passing, G., Schonfelder, H. and Brook, R. J., Synthesis of dense silicon-based ceramics at low temperatures. *Nature*, 1992, **355**(6362), 714–717.
8. Zhu, X. W., Jiang, D. L. and Tan, S. L., Preparation of silicon carbide reticulated porous ceramics. *Mater. Sci. Eng.*, 2002, **A323**(1–2), 232–238.
9. Jiang, D. L. and Zhu, X. W., Preparation and properties of silicon carbide reticulated porous ceramics. *Key Eng. Mater.*, 2003, **247**, 19–26.
10. She, J. H. and Deng, Z. Y., Oxidation bonding of porous silicon carbide ceramics. *J. Mater. Sci.*, 2002, **37**(17), 3615–3622.
11. She, J. H., Ohji, T. and Kanzaki, S., Oxidation bonding of porous silicon carbide ceramics with synergistic performance. *J. Eur. Ceram. Soc.*, 2003, **24**(21), 331–334.
12. She, J. H. and Ohji, T., Thermal shock behavior of porous silicon carbide ceramics. *J. Am. Ceram. Soc.*, 2002, **85**(8), 2125–2127.
13. Wu, S., Chan, H. M. and Harmer, M. P., Reaction-forming of mullite ceramics using an aqueous milling medium. *J. Am. Ceram. Soc.*, 1997, **80**(6), 1579–1582.
14. Touloukian, Y. S., *Thermophysical Properties of Matter*, *vol. 13*. IFI/Plenum Data Company Press, New York, 1979.

15. Ding, S., Zhu, S., Zeng, Y. and Jiang, D., Effect of $Y_2O_3$ addition on the properties of reaction-bonded porous SiC ceramics. *Ceram. Int.*, 2006, **32**(4), 461–466.
16. Jorgensen, P. J., Wadsworth, M. E. and Cutler, I. B., Oxidation of silicon carbide. *J. Am. Ceram. Soc.*, 1959, **42**(12), 613–616.
17. Ervin, G., Oxidation behavior of silicon carbide. *J. Am. Ceram. Soc.*, 1958, **41**(9), 347–352.
18. Aksay, I. A. and Pask, J. A., Stable and metastable phase equilibria in the system $Al_2O_3/SiO_2$. *J. Am. Ceram. Soc.*, 1975, **58**(11–12), 507–512.
19. Davis, R. F. and Pask, J. A., Diffusion and reaction studies in the system $Al_2O_3$–$SiO_2$. *J. Am. Ceram. Soc.*, 1972, **55**(10), 525–531.
20. Mechnich, P., Scheider, H., Schmucker, M. and Saruhan, B., Accelerated reaction bonding of mullite. *J. Am. Ceram. Soc.*, 1998, **81**(7), 1931–1937.
21. Saruhan, B., Albers, W., Schneider, H. and Kaysser, W. A., Reaction and sintering mechanisms of mullite in the systems cristobalite/$\alpha$-$Al_2O_3$ and amorphous $SiO_2$/$\alpha$-$Al_2O_3$. *J. Eur. Ceram. Soc.*, 1996, **16**, 1075–1081.
22. Nurishi, Y. and Pask, J. A., Sintering of $\alpha$-$Al_2O_3$ amorphous silica compacts. *Ceram. Int.*, 1982, **8**, 57–59.
23. Scheppokat, S., Janssen, R. and Claussen, N., Phase development and shrinkage of reaction-bonded mullite composites with silicon carbide of different particle sizes. *J. Am. Ceram. Soc.*, 1999, **82**(2), 319–324.
24. Lange, F. F., Deformation consolidation of metal powders containing steel inclusions. *Acta Mater.*, 1991, **39**(2), 209–219.
25. Obadia, S. and Broussaud, D., *Microstructural developments in $Al_2O_3$-$SiO_2$ sintered ceramics for high temperature application. In Science of Ceramics, vol. 14*, ed. D. Taylor. Institute of Ceramics, UK, 1998, pp. 431–436.
26. Greil, P., Vogli, E., Fey, T., Bezold, A., Popovska, N., Gerhard, H. and Sieber, H., Effect of microstructure on the fracture behavior of biomorphous silicon carbide ceramics. *J. Eur. Ceram. Soc.*, 2002, **22**, 2697–2707.
27. Rice, R. W., Comparison of stress concentration versus minimum solid area based mechanical property–porosity relations. *J. Mater. Sci.*, 1993, **28**(8), 2187–2190.
28. Rice, R. W., Grain-size dependence of fracture energy in ceramics. I. Experiment. *J. Am. Ceram. Soc.*, 1981, **64**(6), 345–350.
29. Rice, R. W., Grain-size dependence of fracture energy in ceramics. II. A model for noncubic materials. *J. Am. Ceram. Soc.*, 1981, **64**(6), 350–354.